*Sensors and Materials*, Vol. 30, No. 7 (2018) 1525–1532
MYU Tokyo



S & M 1607

# Scintillation Properties of (Lu,Y)$AlO_3$ Doped with Nd

Masaki Akatsuka,* Yuki Usui, Daisuke Nakauchi,
Go Okada, Noriaki Kawaguchi, and Takayuki Yanagida

Graduate School of Materials Science, Nara Institute of Science and Technology,
8916-5 Takayama, Ikoma, Nara 630-0192, Japan

(Received January 19, 2018; accepted March 2, 2018)

***Keywords:*** scintillation, near infrared, Nd, ceramic

(Lu,Y)$AlO_3$ crystals doped with different concentrations of Nd were synthesized by the floating-zone (FZ) method to evaluate their scintillation properties, particularly in the near-infrared (NIR) range. Under X-ray irradiation, scintillation due to the $^4F_{3/2}\rightarrow{}^4I_{11/2}$ transition of $Nd^{3+}$ was observed at 1064 nm. The scintillation decay time profile was approximated by an exponential decay function, and the obtained value varied from 2–3 to 150 μs depending on the concentration of $Nd^{3+}$.

## 1. Introduction

Scintillators have a function to immediately convert the absorbed energy of ionizing radiation (typically of keV to GeV) to thousands of low-energy photons.[1] The application fields of scintillators are very broad, and they include medical imaging,[2] security,[3] environmental monitoring,[4] and high-energy physics.[5] The scintillators are in various kinds of material forms, such as inorganic/organic solid, liquid, and gas, which affect the scintillation properties. Among them, inorganic solid-state scintillators are the most common. Scintillators are often considered in terms of the density ($\rho$), effective atomic number ($Z_{eff}$), scintillation decay time, afterglow level, light yield, and radiation tolerance. In particular, $\rho$ and $Z_{eff}$ are important for achieving high detection efficiency against high-energy photons since the probability of photoelectric interaction events with the material is proportional to $\rho Z_{eff}^4$. In reality, there is no ideal scintillator to fulfill all the properties required for all the applications; therefore, users must select suitable scintillators for their purposes. Among many inorganic scintillators, garnet materials have, in particular, superior fluorescence properties, and many studies have been performed to investigate their scintillation properties.[6,7]

Recently, scintillators emitting near-infrared (NIR) photons have attracted much attention because a human body can transmit NIR photons.[8–12] Since there is an optical window from 700–1200 nm in the human body, the scintillator materials emitting NIR photons can be used for bioimaging. For example, in radiation therapy, a small NIR scintillator is embedded in the affected part of the human body so that it emits NIR light when radiation is delivered to the

*Corresponding author: e-mail: akatsuka.masaki.ad5@ms.naist.jp
http://dx.doi.org/10.18494/SAM.2018.1922

ISSN 0914-4935 

appropriate part. The NIR scintillation can be transmitted through the optical window of the patient's body; therefore, the scintillation signal can be detected by a photodetector in real time in order to ensure the appropriate radiation delivery. In addition, the photon energies of NIR quanta are approximately 1 eV lower than those of UV or VIS light; therefore, NIR-emitting scintillators are considered to have a higher scintillation light yield, which is the number of scintillation photons per absorbed energy of ionizing radiation. Furthermore, in high-dose environments (e.g., nuclear reactors), we expect such NIR-emitting scintillators to be effective tools for monitoring radiation dose. In general, scintillation detectors for monitoring high radiation doses are a combination of a scintillator and optical fiber. However, the optical fiber suffers from radiation damage and the UV–VIS light transmittance is degraded,[13] strongly weakening the scintillation emission if the scintillator emission is in the UV–VIS range. On the other hand, NIR-emitting scintillators are useful in such a measurement configuration because the radiation damage has no effect in the NIR range. Despite such usefulness, there have been only a few reports on NIR-emitting scintillators, and there remains much room for studying this topic. One reason is that the conventional Si-based photodetectors do not have sufficient sensitivity of emission with wavelengths longer than 800 nm, so in previous studies, only emissions up to 800 nm could be characterized.[14,15] Recently, on the other hand, we have dramatically expanded the spectral range of measurement by using an InGaAs-based detector to study NIR-emitting scintillators for bioimaging and high-dose-monitoring applications. Up to now, we have reported NIR scintillations (600–1650 nm) in oxide garnets ($Nd^{3+}$-doped), sesquioxides ($Yb^{3+}$-doped $Lu_2O_3$), and fluorides ($Nd^{3+}$-doped $YLiF_4$).[16–20]

Most inorganic crystalline scintillators of oxides and fluorides have superior scintillation characteristics. In order to extend the investigation on NIR-emitting scintillators, in this study, we focused on Nd-doped (Lu,Y)$AlO_3$ [grown by the floating-zone (FZ) method] since most garnet materials have been intensively studied, while perovskite materials are also suitable for scintillator uses. As the perovskite host, we selected (Lu,Y)$AlO_3$ since $\rho$ and $Z_{eff}$ of common $YAlO_3$ [yttrium aluminum perovskite (YAP)] are not sufficiently high for scintillators. The Nd was added as an emission center for NIR emission since $Nd^{3+}$ is known to be a luminous emission center, especially in laser applications. The obtained crystals were evaluated in terms of photoluminescence (PL), scintillation, and thermoluminescence (TL) properties.

## 2. Experimental Procedure

Nd-doped (Lu,Y)$AlO_3$ (Nd = 0.1, 0.3, 1.0, 3.0, 10 mol.%) samples were synthesized by the FZ method. Here, the ratio of Lu to Y was fixed to Lu:Y = 1:1, and Nd was added as a substitute for lutetium. In addition, we prepared Nd-free (Lu,Y)$AlO_3$ for comparison. The raw material powders used were $Lu_2O_3$ (5N), $Al_2O_3$ (4N), $Y_2O_3$ (4N), and $Nd_2O_3$ (4N). They were mixed to the compositions as above. After mixing, the powders were formed into a cylindrical rod by applying hydrostatic pressure. After the shaping process, the cylinders of all the compositions were sintered at 1100 °C for 8 h in air to obtain ceramic rods. Finally, we conducted crystal growth by melting the ceramic rod via the FZ method in air. The FZ furnace used was Canon Machinery FZD0192. Here, the rotation rate was 20 rpm, and the pull-down rate was 2.5–5 mm/h.

The PL excitation/emission contour spectrum (or PL map) and PL quantum yield (*QY*) were measured using Quantaurus-QY (C11347, Hamamatsu). The excitation and emission wavelength ranges for the PL map were 250–800 and 300–950 nm, respectively. The measurement interval for excitation wavelength was 10 nm. The absolute *QY* was calculated as $QY = N_{emit}/N_{absorb}$, where $N_{emit}$ and $N_{absorb}$ are the numbers of emitted and absorbed photons, respectively. PL decay time profiles were evaluated using Quantaurus-τ (C11367, Hamamatsu), and the excitation and monitoring wavelengths were selected on the basis of the obtained PL map.

The scintillation spectra were evaluated at room temperature under X-ray irradiation in our original setup.[21] The excitation source was an X-ray generator (XRB80N100, Spellman) equipped with a conventional X-ray tube, supplied with 40 kV bias voltage and 1.2 mA tube current. The emission spectra were measured using two different spectrometers to cover a wide spectral range from UV to NIR: Andor Newton 920 for 180–700 nm and Andor iDUS for 650–1650 nm. The CCDs of the Andor spectrometers were cooled to 193 K using a Peltier device to reduce thermal noise. In order to avoid the CCD being exposed directly to X-rays, the spectrometers were placed off the irradiation axis, and the scintillation light was fed into the spectrometers through 2 m of optical fiber. The scintillation decay time profiles were also evaluated in our original setup.[22] In addition, a previous report indicated that YAP showed very strong TL;[23] therefore, we also evaluated the TL glow curve by heating a sample at a constant rate (1 °C/s) over 50 to 490 °C, using a TL reader (TL-2000, Nanogray).[24]

## 3. Results and Discussion

### 3.1 Sample appearance

As-synthesized rods were typically 4 mm in diameter and 15–20 mm in length. These rods were cut into pieces for characterization. Figure 1 shows the samples used for characterization. The Nd-free and 0.1–3.0% Nd-doped samples looked opaque, indicating that these samples are in a ceramic (or polycrystalline) form. However, the 10% Nd-doped sample looked transparent, so we conclude that this was grown in a single crystal.

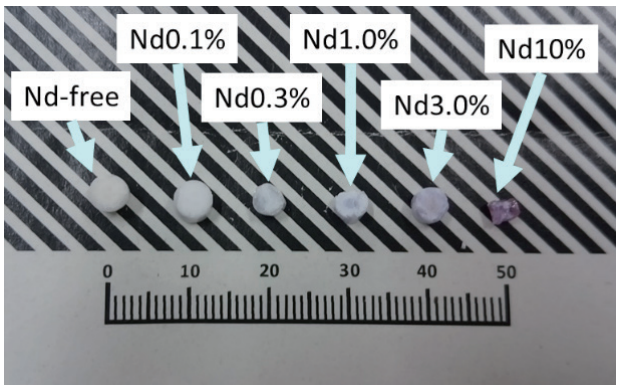


Fig. 1. (Color online) Photograph of $(Lu,Y)AlO_3$ samples doped with different concentrations of Nd.

Figure 2 shows the powder X-ray diffraction (XRD) patterns of prepared samples. All the diffraction patterns measured corresponded well with the standard crystallographic data (JCPDS Nos. 871290, 240690, 330844, and 731368). Moreover, $LuAlO_3$ and $YAlO_3$ have the same crystal structure and very similar XRD patterns; therefore, we used $(Lu,Y)AlO_3$. The 10% Nd-doped sample seems to have a perovskite single-crystal layer. On the other hand, the Nd-free and 0.1–3.0% Nd-doped samples seem to have not only the perovskite structure but also garnet and monoclinic structures. In this result, we considered that, in general, the mixed crystal of $Lu_4Al_2O_9$ and $Lu_3Al_5O_{12}$ is easier to grow than the $(Lu,Y)AlO_3$ single crystal. However, the (f) sample was doped with a large amount of Nd compared with other samples and we considered that the large amount of Nd facilitated the growth of the perovskite structure. Thus, the (f) sample was grown as a $(Lu,Y)AlO_3$ single crystal. From the viewpoint of the diffraction angle, the diffraction angles of 0.1–3.0% Nd-doped samples are the same as that of the Nd-free sample. Thus, it is expected that Nd cations will mainly exist in the interface of crystallites.

### 3.2 PL properties

Figure 3 shows the PL emission map of 1.0% Nd-doped $(Lu,Y)AlO_3$ as a representative example. It shows strong emission at around 900 nm owing to the 4f–4f transitions of $Nd^{3+}$.[25] Here, the integrated emission range was from 800 to 950 nm for all samples. As a result, *QY* values of Nd-free, 0.1, 0.3, 1.0, 3.0, and 10.0% samples were 0, 26.9, 28.2, 22.1, 9.3, and 0.3%, respectively. Among all the samples, the 0.3% Nd-doped sample showed the highest *QY* value, and the 10% Nd-doped sample showed very low *QY*, although it had a high transparency. We consider that the 10% Nd-doped sample suffered from concentration quenching. The well-known intense emission of $Nd^{3+}$ at 1064 nm is not included because our apparatus cannot measure photons of wavelengths larger than 960 nm.

The PL decay curves of the Nd-doped samples are illustrated in Fig. 4. Here, the monitoring wavelength was around 900 nm. The excitation wavelength was selected to be the one at which the *QY* is the highest. All the decay curves followed a simple exponential decay function. The Nd-free sample did not show any signal. For the 0.1–3.0% Nd-doped samples, the PL decay

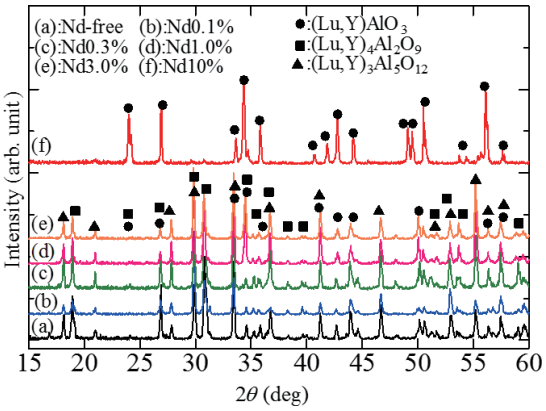


Fig. 2. (Color online) Powder XRD patterns of (Lu,Y)$AlO_3$ doped with different concentrations of Nd.

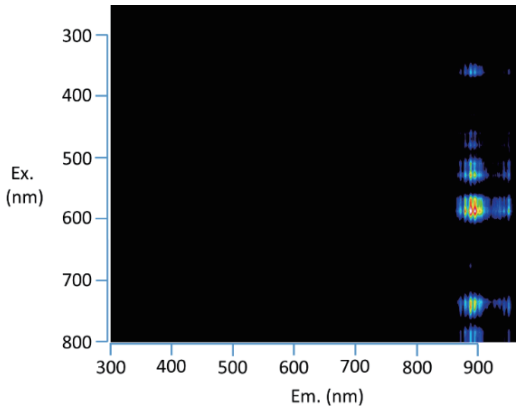


Fig. 3. (Color online) PL map of 0.3% Nd-doped $(Lu,Y)AlO_3$. The horizontal and vertical axes show emission and excitation wavelengths, respectively.

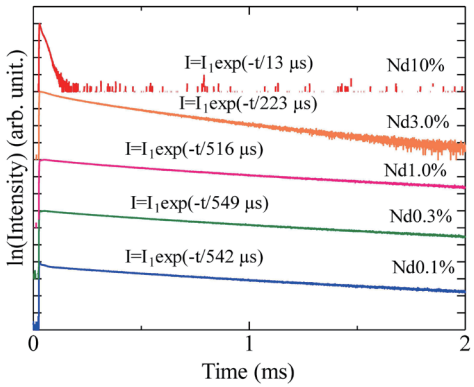


Fig. 4. (Color online) PL decay curves of $(Lu,Y)AlO_3$ doped with different concentrations of Nd. The monitoring wavelength was around 900 nm.

time of 4f–4f transitions of $Nd^{3+}$ was 220–550 μs. These decay times were typical for the 4f–4f transitions of $Nd^{3+}$ and agreed with the values reported in previous studies.[25–27] The decay time of the 10% Nd-doped sample was very short. This finding supports the idea that the 10% Nd-doped sample suffered from concentration quenching. Furthermore, the decay time of the 3.0% Nd-doped sample was shorter than those of the 0.1–1.0% Nd-doped samples. Therefore, the 3.0% Nd-doped sample also possibly suffered from concentration quenching.

### 3.3 Scintillation properties

Figure 5 shows X-ray-induced scintillation spectra measured in the (a) UV–VIS and (b) NIR ranges. The Nd-free sample showed emission at around 300 nm. In previous studies, nondoped $YAlO_3$ and $Y_3Al_5O_{12}$ showed emission at around 300 and 355 nm owing to lattice defects, respectively.[28] For the Nd-doped samples, the 4f–4f transitions of $Nd^{3+}$ were observed in the UV–VIS range, which were not observed in PL. The emission features were typical and can be identified as the electronic transitions of $^2F_{5/2}\rightarrow{}^4F_{5/2}$ (400 nm), $^2F_{5/2}\rightarrow{}^4F_{9/2}$ (450 nm), $^2F_{5/2}\rightarrow{}^4G_{5/2}$ (480 nm), $^2F_{5/2}\rightarrow{}^4G_{7/2}$ (540 nm), and $^2F_{5/2}\rightarrow{}^4G_{9/2}$ (550 nm).[16,19,29,30] In the NIR range, all the Nd-doped samples showed emissions due to the electronic transitions of $^4F_{3/2}\rightarrow{}^4I_{9/2}$ (910 nm), $^4F_{3/2}\rightarrow{}^4I_{11/2}$ (1064 nm), and $^4F_{3/2}\rightarrow{}^4I_{13/2}$ (1320 nm). The emission of 1064 nm is well known for laser applications,[31] and the emission intensities of 0.1–3.0% Nd-doped samples were high. Although the intensity of the integrated scintillation dealt with here is qualitative (unlike in the case of the pulse-counting technique), the 0.3% Nd-doped sample showed the strongest NIR emission intensity. The emission of the 10% Nd-doped sample was very weak, which was consistent with the results of PL.

Figure 6 shows X-ray-induced scintillation decay time profiles of Nd-doped $(Lu,Y)AlO_3$. The decay curves of the 0.1–3.0% Nd-doped samples were approximated as the sum of two exponential decay functions, and the faster decay component was considered to be a tail of the instrumental response (~10 μs) while the longer component was considered to be the signal from the sample. In contrast, the 10% Nd-doped sample was approximated by a single exponential decay function. These components were due to the 4f–4f transitions of $Nd^{3+}$. These decay times, except for the 10% Nd-doped sample, were typical values of the 4f–4f transitions of

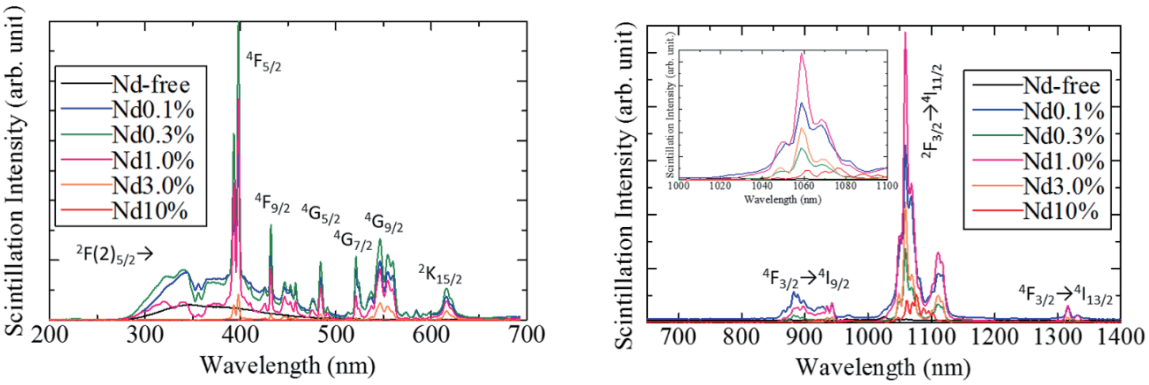


(a) (b)

Fig. 5. (Color online) X-ray-induced scintillation spectra of $(Lu,Y)AlO_3$ doped with different concentrations of Nd in the (a) UV–VIS and (b) NIR ranges.

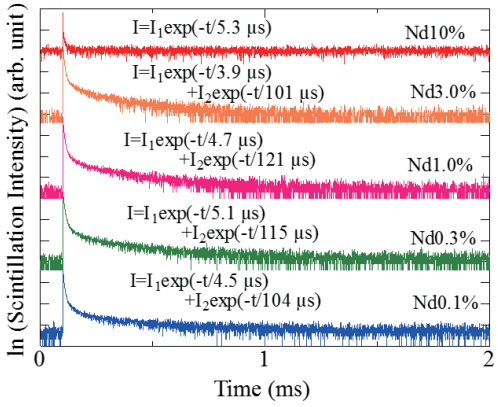


Fig. 6. (Color online) X-ray-induced scintillation decay time profiles of $(Lu,Y)AlO_3$ doped with different concentrations of Nd. The monitoring wavelength was 400–900 nm.

$Nd^{3+}$ reported from previous studies.[17–19] In general, the scintillation phenomenon consists of three different processes: generation of electrons and holes, energy transport, and emission at luminescence centers. Therefore, the scintillation decay time is generally slower than that of PL. However, the scintillation decay times of all the samples were faster than those of PL in our materials. A possible reason is some kind of quenching among secondary electrons generated by X-ray irradiation. The same behavior was observed in different phosphors reported elsewhere.[32,33]

### 3.4 TL properties

Figure 7 shows TL glow curves of $(Lu,Y)AlO_3$ doped with different concentrations of Nd. The glow curves were measured after irradiating the samples with X-rays of 0.1 Gy. The Nd-free and 0.1% Nd-doped samples demonstrate glow peaks at around 150 and 300 °C. However, the glow peaks of the 0.1% Nd-doped sample are weaker than those of the Nd-free sample, and

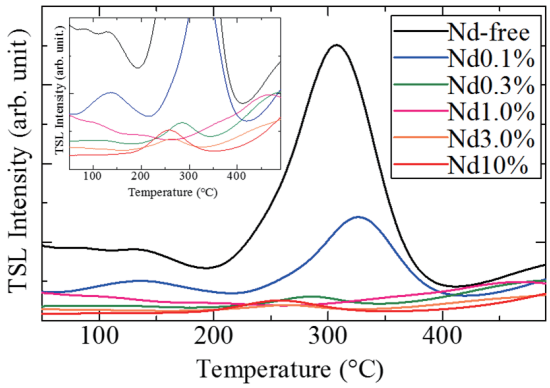


Fig. 7. (Color online) TL glow curves of (Lu,Y)AP doped with different concentrations of Nd. The samples were irradiated with X-rays of 0.1 Gy before measurement. The monitored wavelength was 250–550 nm.

the samples doped with 0.3% or more Nd showed small glow peaks. This tendency was the same as those in Eu-doped $YAlO_3$.[23] It is suggested that, in the Nd-doped samples, most of the energy of secondary electrons excited by X-ray irradiation was transferred to the scintillation. In addition, the 10% Nd-doped sample shows neither scintillation nor TL. In both scintillation and TL, the final luminescence process depends on *QY*. Thus, the 10% Nd-doped sample, which showed a very low *QY*, should not show intense emission.

## 4. Conclusions

We synthesized Nd-doped (Lu,Y)$AlO_3$ by the FZ method to evaluate their PL, scintillation, and TL properties. For scintillation, the 0.1–3.0% Nd-doped samples demonstrated a strong emission peak at 1064 nm owing to $^4F_{3/2} \rightarrow {}^4I_{11/2}$ transitions of $Nd^{3+}$. The latter decay time was of a typical order; however, that of PL was longer than that of scintillation. This finding suggests that some sort of quenching took place during the scintillation process. For TL properties, the Nd-free sample exhibited the strongest glow peak among all the samples, and the origin of this emission would be due to the host since a similar glow curve was observed in $YAlO_3$.

## Acknowledgments

This work was supported by Grant-in-Aid for Scientific Research (A) (17H01375) and Grant-in-Aid for Young Scientists (B) (17K14911) from the Ministry of Education, Culture, Sports, Science and Technology of the Japanese government (MEXT) as well as A-STEP from the Japan Science and Technology Agency (JST). The Cooperative Research Project of the Research Institute of Electronics, Shizuoka University, Mazda Foundation, Konica Minolta Science and Technology Foundation, Taisei Foundation, SEI Group CSR Foundation, NAIST Foundation, and TEPCO Memorial Foundation are also acknowledged.

## References


1 T. Yanagida: Opt. Mater. **35** (2013) 1987.
2 S. Yamamoto, K. Kuroda, and M. Senda: IEEE Trans. Nucl. Sci. **50** (2003) 1683.
3 J. Glodo, Y. Wang, R. Shawgo, C. Brecher, R. H. Hawrami, J. Tower, and K. S. Shah: Phys. Proc. **90** (2017) 285.
4 S. Moriuchi, M. Tsutsumi, and K. Saito: Jpn. J. Health Phys. **44** (2007) 122.
5 T. Ito, M. Kokubun, T. Takashima, T. Yanagida, S. Hirakuri, R. Miyawaki, H. Takahashi, K. Makishima, T. Tanaka, K. Nakazawa, T. Takahashi, and T. Honda: IEEE Trans. Nucl. Sci. **53** (2006) 2983.
6 T. Yanagida, K. Watanabe, Y. Fujimoto, A. Uritani, H. Yagi, and T. Yanagitani: J. Ceram. Soc. Jpn. **122** (2014) 1016.
7 D. Nakauchi, G. Okada, N. Kawano, N. Kawaguchi, and T. Yanagida: Appl. Phys. Express **10** (2017) 072601.
8 Y. Huang, M. Hamblin, and A. C.-H. Chen: SPIE (2009). doi:10.1117/2.1200906.1669
9 R. Weissleder: Nat. Biotechnol. **19** (2001) 316.
10 C. Amiot, S. Xu, S. Liang, L. Pan, and J. Zhao: Sensors **8** (2008) 3082.
11 K. Soga, T. Tsuji, F. Tashiro, J. Chiba, M. Oishi, K. Yoshimoto, Y. Nagasaki, K. Kitano, and S. Hamaguchi: J. Phys. Conf. Ser. **106** (2008) 012.
12 J.-L. Boulnois: Lasers Med. Sci. **1** (1986) 4766.
13 K. Toh, T. Nakamura, H. Yamagishi, K. Sakasai, K. Soyama, and T. Shikama: Nucl. Instrum. Methods Phys. Res., Sect. A **700** (2013) 130.
14 W. W. Moses, M. J. Weber, S. E. Derenzo, D. Perry, P. Berdahl, and L. A. Boatner: IEEE Trans. Nucl. Sci. **45** (1998) 462.
15 P. A. Rodnyi, E. I. Gorohova, S. B. Mikhrin, A. N. Mishin, and A. S. Potapov: Nucl. Instrum. Methods Phys. Res., Sect. A **486** (2002) 244.
16 T. Yanagida and H. Sato: Opt. Mater. **38** (2014) 174.
17 T. Yanagida, Y. Fujimoto, H. Yagi, and T. Yanagitani: Opt. Mater. **36** (2014) 1044.
18 T. Yanagida, Y. Fujimoto, S. Ishizu, and K. Fukuda: Opt. Mater. **41** (2015) 36.
19 T. Oya, G. Okada, and T. Yanagida: J. Ceram. Soc. Jpn. **124** (2016) 536.
20 G. Okada, N. Kawaguchi, and T. Yanagida: Sens. Mater. **29** (2017) 1407.
21 T. Yanagida, K. Kamada, Y. Fujimoto, H. Yagi, and T. Yanagitani: Opt. Mater. **35** (2013) 24802.
22 T. Yanagida, Y. Fujimoto, T. Ito, K. Uchiyama, and K. Mori: Appl. Phys. Express **7** (2014) 062401.
23 T. Kuro, D. Nakauchi, G. Okada, N. Kawaguchi, and T. Yanagida: Opt. Mater. **64** (2017) 282.
24 T. Yanagida, Y. Fujimoto, N. Kawaguchi, and S. Yanagida: J. Ceram. Soc. Jpn. **121** (2013) 989.
25 H. S. Möller, A. Hoffmann, D. Knaut, J. Flottmann, and T. Jüstel: J. Lumin. **158** (2015) 365.
26 H. Yagi, T. Yanagitani, K. Takaichi, K. Ueda, and A. A. Kaminskii: Opt. Mater. **29** (2007) 1258.
27 J. Lu, M. Prabhu, J. Song, C. Li, J. Xu, K. Ueda, A. A. Kaminskii, H. Yagi, and T. Yanagitani: Appl. Phys. B **71** (2000) 469.
28 V. Mürk, A. Kuznetsov, B. Namozov, and K. Ismailov: Nucl. Instrum. Methods Phys. Res., Sect. B **91** (1994) 327.
29 S. M. Reda, C. R. Varney, and F. A. Selim: Res. Phys. **2** (2012) 123.
30 L. Ninga, P. A. Tannera, V. V. Harutunyanb, E. Aleksanyan, V. N. Makhov, and M. Kirm: J. Lumin. **127** (2007) 397.
31 X. D. Xu, X. D. Wang, J. Q. Meng, Y. Cheng, D. Z. Li, S. S. Cheng, F. Wu, Z. W. Zhao, and J. Xu: Laser Phys. Lett. **6** (2009) 678.
32 T. Yanagida and G. Okada: J. Ceram. Soc. Jpn. **124** (2016) 564.
33 D. Nakauchi, G. Okada, M. Koshimizu, and T. Yanagida: J. Lumin. **176** (2016) 342.